Peroxynitric acid (HO_2NO_2) measurements during the UBWOS 2013 and 2014 studies using iodide ion chemical ionization mass spectrometry.

Patrick R. Veres[a,b,*], James M. Roberts[b], Robert J. Wild[a,b], Peter M. Edwards[a,b,c], Steven S. Brown[b], Timothy S. Bates[d,e], Patricia K. Quinn[e], James E. Johnson[d], Robert J. Zamora[f], Joost de Gouw[a,b]

[a]Cooperative Institute for Research in Environmental Sciences, University of Colorado, Boulder, Colorado, USA
[b]Chemical Sciences Division, NOAA Earth System Research Laboratory, Boulder, CO, USA
[c]Now at Department of Chemistry, University of York, York, YO10 5DD, UK
[d]Joint Institute for the Study of the Oceans and Atmosphere, University of Washington, Seattle, WA, USA
[e]NOAA PMEL, Seattle, WA, USA
[b]Physical Sciences Division, NOAA Earth System Research Laboratory, Boulder, CO, USA
[*]Correspondence to: patrick.veres@noaa.gov

Abstract

Laboratory work is reported here establishing iodide ion chemical ionization mass spectrometry (I^- CIMS) as a sensitive method for the unambiguous detection of peroxynitric acid (HO_2NO_2, PNA). A dynamic calibration source for HO_2NO_2, HO_2, and HONO was developed and calibrated using a novel total NO_y detector (NO_y CaRDS). Photochemical sources of these species were used for the calibration and validation of the I^- CIMS instrument for detection of HO_2NO_2. Ambient observations of HO_2NO_2 using I^- CIMS were made during the 2013 and 2014 Uintah Basin Wintertime Ozone Study (UBWOS) are presented. Strong inversions leading to a build-up of many primary and secondary pollutants as well as low temperatures drove daytime HO_2NO_2 as high as 1.5 ppbv during the 2013 study. A comparison of HO_2NO_2 observations to mixing ratios predicted using a chemical box model describing an ozone formation event observed during the 2013 wintertime shows agreement in the daily maxima HO_2NO_2 mixing ratio, but a differences of several hours in the timing of the observed maxima. Observations of vertical gradients suggest that the ground snow surface potentially serves as both a net sink and source of HO_2NO_2 depending on time of day. Sensitivity tests using a chemical box model indicate that the lifetime of HO_2NO_2 with respect to deposition has a non-negligible impact on ozone production rates on the order of 10%.

1 Introduction

Hydrogen oxides ($HO_x = HO_2 + OH$) and nitrogen oxides ($NO_x = NO_2 + NO$) play central roles in atmospheric photochemistry. HO_2, a product of OH-initiated VOC oxidation, reacts with NO to produce NO_2, a key step in the photochemical ozone formation cycle in the troposphere. Peroxynitric acid (often referred to as PNA, HO_2NO_2, or HNO_4) plays an important role in the coupling of atmospheric HO_x and NO_x cycles (Niki et al., 1977), especially at low temperatures. PNA serves as an important HO_x and NO_x reservoir species altering the oxidative capacity of the atmosphere on regional and global scales (Kim et al., 2007;Chen et al., 2001;Davis et al., 2001;Carpenter et al., 2000).

PNA is formed via the reaction of HO_2 and NO_2 (DeMore et al., 1997;Sander et al., 2011).

$$HO_2 + NO_2 \xrightarrow{M} HO_2NO_2 \qquad (1)$$

Formation via reaction (1) is favored at low temperatures and high pressures (Kim et al., 2007). Unimolecular decomposition is temperature dependent and occurs on a timescale of approximately 10 seconds at 1 atm, 298K with the lifetime rapidly increasing to hours at 258K (Gierczak et al., 2005);

$$HO_2NO_2 \xrightarrow{M} HO_2 + NO_2 \tag{2}$$

PNA can be lost *via* photolysis in the near ultraviolet (Jimenez et al., 2005) and near infrared *via* an overtone band (Roehl et al., 2002;Stark et al., 2008);

$$HO_2NO_2 \xrightarrow{\lambda} OH + NO_2 \tag{3}$$

$$HO_2NO_2 \xrightarrow{\lambda} HO_2 + NO_2 \tag{4}$$

Or by reaction with OH (Jimenez et al., 2004);

$$HO_2NO_2 + OH \longrightarrow H_2O + NO_2 + O_2 \tag{5}$$

In the lower troposphere, reactions (3), (4), and (5) typically occur on timescales of days to months thereby implying that the dominant loss of PNA in the lower troposphere is typically unimolecular dissociation or deposition.

Deposition of PNA on snow surfaces has been observed in various studies where the atmospheric lifetime of PNA in Polar Regions is largely controlled by dry deposition (Huey et al., 2004;Slusher et al., 2002;Jones et al., 2014). Additional laboratory studies have been performed confirming the efficient uptake of PNA to ice (Li et al., 1996;Ulrich et al., 2012) and sulfuric acid solutions (Zhang et al., 1997). Dependent on the fate of PNA after deposition, the formation and subsequent deposition of PNA has been suggested to result in a net loss of HO_x and an increase in NO (Grannas et al., 2007), with reactions (1) to (5) thereby having an impact on tropospheric ozone formation (Salawitch et al., 2002).

Observations of PNA are generally limited in scope with most measurements focusing on polar regions (Slusher et al., 2002;Huey et al., 2004;Slusher et al., 2010), the free troposphere (Murphy et al., 2004;Singh et al., 2006;Singh et al., 2007;Keim et al., 2008;Kim et al., 2007), and the stratosphere (Rinsland et al., 1996;Rinsland et al., 1986;Sen et al., 1998). Mean PNA observations from these studies range from tens of pptv in polar surface regions to several hundred pptv in the upper troposphere/lower stratosphere. The impacts of PNA on upper tropospheric chemistry have been widely discussed (Brune et al., 1999;Wennberg et al., 1999;Faloona et al., 2000), with one study in particular identifying a PNA contribution as high as 20% of the total NO_y budget (Murphy et al., 2004). Lower-tropospheric, mid-latitude measurements, in contrast, remain largely unexplored with the exception of, to our knowledge, a single airborne study conducted in Mexico (Spencer et al., 2009) where PNA concentrations up to 600 pptv were observed, and were correlated with O_3 formation.

The general lack of lower-tropospheric, mid-latitude observations is driven in part by two factors (i) a diminished atmospheric impact of PNA due to higher rates of thermal decomposition with respect to the generally colder polar and upper atmosphere, and (ii) a lack of instrumentation capable of providing sensitive unambiguous measurements of PNA. Many of the techniques available measure PNA as a component of NO_y using O_3/NO chemiluminescence

(Keim et al., 2008) or total peroxynitrates *via* thermal decomposition laser induced fluorescence (Murphy et al., 2004). Currently available instrumentation capable of unambiguous measurement of PNA is limited to remote sensing detection *via* IR absorption spectroscopy (Rinsland et al., 1986;Rinsland et al., 1996;Sen et al., 1998) or in-situ measurement *via* chemical ionization mass spectrometry using the SiF_6^- ion (Slusher et al., 2002;Slusher et al., 2001;Huey, 2007), CF_3O^- (Spencer et al., 2009;Huey et al., 1996), and I^- (Abida et al., 2011). Among these, CIMS techniques have been shown to have sufficient sensitivity and time resolution for the in-situ monitoring of PNA concentrations in the lower troposphere.

In this work, we present laboratory and ambient measurements illustrating the utility of iodide ion CIMS for unambiguous measurement of PNA. Additionally, we show applicability of this technique for the detection of both HO_2 and HONO, atmospheric species that are also integral to HO_x and NO_x cycles. These results were necessary in order to rule out potential mass overlap or PNA interferences from the sampling of HO_2 and HONO. A photo-source has been developed for dynamic production of PNA, HO_2, and HONO to assist with laboratory calibration and elucidation of various ionization schemes. PNA observations made during the 2013 and 2014 Uintah Basin Wintertime Ozone Study (UBWOS) will be presented and compared to the results of a chemically explicit box model developed to describe the air quality in the Uintah Basin during a high ozone event observed during the 2013 study (Edwards et al., 2014). The impact of PNA on HOx and NOx budgets, particularly as it relates to the photochemical production of ozone, will also be discussed.

2 Experimental Setup

We present both laboratory and field data collected over a two-year period encompassing the 2013 and 2014 UBWOS field studies. The following describes the instrumentation used in this work as well as a short description of the UBWOS study and field conditions. Information and links pertaining to the 2013 and 2014 Uintah Basin Winter Ozone Studies are available on the web (http://esrl.noaa.gov/csd/groups/csd7/measurements/2013ubwos/ and http://esrl.noaa.gov/csd/groups/csd7/measurements/2014ubwos/).

2.1 Instrumentation

2.1.1 Iodide Ion CIMS (I^- CIMS)

The I^- CIMS instrument consists of an ion flow tube coupled to a quadrupole mass spectrometer. Briefly, CH_3I in N_2 is passed through a ^{210}Po ionizer resulting in the production of iodide (I^-) ions. Subsequently, I^- reacts in the flow tube with a sample gas resulting in the production of anions that are mass filtered using a quadrupole mass spectrometer and detected. Additional details about the instrument can be found elsewhere (Slusher et al., 2004). The instrumental differences with respect to that described in Slusher et al. 2004 will be discussed as they relate to the field deployments and laboratory measurements presented.

The sensitivity of the I^- CIMS to the species presented in this work (HO_2NO_2, HONO, and HO_2) is dependent on the degree of water clustering present in the flow tube. Some ionization reactions occur faster through the $I\text{-}H_2O^-$ cluster, likely as a result of ligand switching *via* an intermediate cluster ion, while other reactions are independent of the water cluster population. A detailed discussion of iodide-water cluster distributions and subsequent effect on the iodide ion CIMS chemistry can be found in the supplementary material of Lee et al. 2014 (Lee et al., 2014). Even with a declustering region present, the ratio of the first water cluster to the parent ion is a valuable diagnostic and can often be a more appropriate way to account for changes in the primary ion signal through normalization of measured signals to the sum of I^- and $I\text{-}H_2O^-$, as was performed in this work.

The extent of the ion clustering in the I^- CIMS can be controlled using a collisional dissociation chamber and through addition of water directly into the flow tube to modify the expected ionization chemistry. This was achieved by flowing ~ 10 sccm N_2 bubbled through water directly into the flow tube at a pressure of 30 torr. In this study, the ratio of the iodide water cluster ion ($I\text{-}H_2O^-$, m/z 145) to the iodide ion (I^-, m/z 127) ranged from approximately 5% to 50% and was adjusted to maximize the instrument sensitivity towards individual species or classes of compounds depending on the application. I^- CIMS was operated in the laboratory with a switchable inlet to allow for sampling through a section of PFA tubing (0.025 m) either at room temperature ('cold') or operated as an inlet dissociator (130ºC, 'hot').

The inlet configuration used during the 2014 UBWOS study was identical to that used in the laboratory experiments, where inlet switching could be performed to sample from either a 'cold' or 'hot' inlet. During the 2013 UBWOS study, however, the I^- CIMS did not employ a switchable inlet; rather a 'hot' inlet dissociator at 150ºC was used throughout the entire measurement period. Never-the-less post experiment tests with the inlet configuration used during UBWOS 2013 permit us to quantify HO_2NO_2 during that study, albeit with increased uncertainty.

2.1.2 Total NO_y Cavity Ring Down Instrument

A novel four channel laser diode based cavity ring-down (CRD) instrument was used to quantify NO, NO_2 and NO_y, during the laboratory portion of this work. Details of the NO_y CRD instrumentation can be found elsewhere (Wild et al., 2014). Briefly, NO_y is thermally dissociated to NO and NO_2 in a heated quartz inlet. Any NO in the sample air or formed *via* catalysis is converted to NO_2 by addition of O_3 after the quartz converter. Quantification of NO_2 in the sample is performed using cavity ring-down at 405 nm.

The quartz converter is typically operated with a gas temperature of 720ºC, however, the temperature can be adjusted downward to measure specific classes of compounds or individual species that contribute to total NO_y while excluding unwanted interferences. A similar method has been used previously for the speciation of NO_y in both ambient and field measurements (Wooldridge et al., 2010;Day et al., 2002). In our experiments, the gas temperature in the converter was optimized for detection of PNA and HONO, 130ºC and 720ºC respectively, a set point determined by scanning the quartz heater through the entire temperature range as shown in Wild et al. 2014 (Wild et al., 2014). A detailed discussion on the application of this technique towards the quantification of HONO and PNA generated in a dynamic laboratory calibration source is included below.

2.2 Field Site Description

The I^- CIMS instrument was deployed during the 2013 and 2014 UBWOS field studies conducted in the Uintah Basin, UT. The goal of these studies was to improve our understanding of the chemistry leading to wintertime observations of elevated ozone levels within the basin. The field site configuration in 2014 is best described by the UBWOS 2012 field report (Lyman and Shorthill, 2012) where a nearly identical site design was employed while a detailed description of the 2013 measurements is available in the UBWOS 2013 field report (Stoeckenius and McNally, 2014).

During both the 2013 and 2014 studies, observations of HO_2NO_2 gradients over snow were conducted by using a moveable (7m, 35ºC) PFA inlet during the 2013 study and a switchable dual inlet system (each inlet was 20m, 30ºC) for the 2014 study. The total inlet flow used during the 2014 study was approximately 20 slpm from which the I^- CIMS subsampled 2 slpm. During the 2013 study, a total inlet flow of 2 slpm was sampled through a short stainless steel section attached to the end of a PFA inlet and heated to a temperature of 65ºC, to dissociate N_2O_5 prior to sampling preventing $ClNO_2$ interferences due to reactions on the inlet surface (Behnke et al., 1997). In this inlet, HO_2NO_2 will dissociate as well as recombine, considering the stability of HO_2 on PFA surfaces. The CIMS instrument in 2013 was not configured to monitor the $I\text{-}HO_2^-$ or $I\text{-}HO_2NO_2^-$ ions, however, NO_3^-, routinely monitored for diagnostic purposes, provides a means to estimate ambient HO_2NO_2 as a result of the large sensitivity of the CIMS to HO_2NO_2 at this ion.

In addition to gas phase measurements conducted at the field site, snow samples were collected daily throughout the UBWOS 2013 and 2014 study. Surface samples were collected from the top 3 cm of snow from undisturbed locations within 1.3km of the field site. At each site, 2 to 6 1L glass jars were collected and kept frozen until analysis, typically within 48 hours of sampling. Prior to analysis *via* an ion chromatograph (IC), samples were melted and filtered using a 25mm diameter 0.4μm pore size nucleopore filter. Filtered samples were subsequently injected directly into the IC and analyzed for anions (e.g. Cl^-, NO_2^-, NO_3^-) and cations (e.g. Na^+, NH_4^+, K^+).

3 Laboratory Results

Laboratory experiments using I^- CIMS were preformed both in preparation and upon the conclusion of the UBWOS 2014 study. The goal of these experiments was to adapt the I^- CIMS technique for the sensitive detection of PNA and develop a method for calibration. The development of an HO_2 based photolysis source for the production of HO_2NO_2 also led to the recognition that the I^- CIMS can be applied to the direct measurement of HO_2 radicals. Additionally, the HO_2 photolysis source is readily adaptable for the production of an on-line HONO calibration standard. These laboratory developments in calibration standard production and I^- CIMS detection of PNA, HONO, and HO_2 will be discussed in detail in the following sections.

3.1 Standard Generation and Detection

The following describes the ion molecule reactions with I^- ions resulting in the detection of HO_2NO_2, HONO and HO_2:

$$I^- + HO_2 \longrightarrow I \bullet HO_2^- \qquad (5)$$

$$I^- + HO_2NO_2 \longrightarrow I \bullet HO_2NO_2^- \qquad (6)$$

$$I^- + HO_2NO_2 \longrightarrow HOI + NO_3^- \qquad (7)$$

$$HO_2NO_2 \xrightarrow{\Delta} HO_2 + NO_2 \xrightarrow{I^-} I \bullet HO_2^- \qquad (8)$$

$$I^- + HONO \longrightarrow I \bullet HONO^- \qquad (9)$$

where reaction (6) is only observed using a 'cold' inlet while reaction (8) occurs upon thermal dissociation of PNA in the inlet. Experimentally, the above reactions, with the exception of reaction (7), were observed in this work to occur predominantly *via* reaction of the hydrated iodide cluster ($I\text{-}H_2O^-$, m/z 145) based on the strong dependence of sensitivity on water vapor observed during these experiments. This implies that the above reactions are ligand switching reactions made faster by the ability of H_2O to accommodate excess energy of reaction through extra degrees of freedom up to and including dissociation.

Normalized (10^6 cps I^-), background corrected mass spectra are shown in Figure 1 for each of the sources. The ratio of m/z 145 ($I\text{-}H_2O^-$) to m/z 127 (I^-) is displayed as a percentage on each panel for reference. These spectra represent the result of the subtraction of a normalized background mass spectrum from a sample spectrum. The background correction method that was applied varies for each species and is dependent on the sample matrix, which will be described separately in the following sections. In all cases, the mass ranges from 126 to 128 and 144 to 146 corresponding to the I^- (m/z 127) and $I\text{-}H_2O^-$ (m/z/ 145) ions were removed to simplify interpretation of the mass spectra. These spectra allow for the identification of impurities in the photolysis sources used as well as demonstrating the ions that were used for the unambiguous detection of each analyte. Each of these sources will be discussed in detail in the following sections.

3.1.1 HO_2 Radical

HO_2 radicals are generated in the laboratory *via* photolysis of H_2O in the presence of O_2 (Dusanter et al., 2008). A mixture of approximately 100 sccm N_2 and 0.5 sccm O_2 was bubbled through water and diluted into a 5 slpm flow of N_2. The mixture is subsequently passed into a PFA photolysis cell and irradiated with a 185 nm Pen-Ray® lamp. The N_2 dilution flow is produced using boil off from a high-pressure liquid nitrogen Dewar to limit the amount of NO_x and VOC in the system. Detection of HO_2 *via* I^- CIMS occurs through direct observation of the parent ion cluster (I-HO_2), therefore, it is not necessary to add CO in order to titrate OH as no measurement interference is expected. Addition of trace amounts of CO was found to increase the concentration of HO_2 produced, though trace amounts of NO and NO_2 from the steel cylinder mixture resulted in an increase in PNA and HONO backgrounds with increasing CO.

Figure 1a shows the difference mass spectrum of the HO_2 radical mixture less the instrument background. In this case, the instrument background was the ion signal measured prior to turning on the 185 nm lamp. It is clear from the mass spectrum that there is only a single dominant peak observed at m/z 160 (I-HO_2^-). A method for the quantitative calibration of the HO_2 radical source and the I^- CIMS instrument for the detection of HO_2 radicals will be discussed in section 3.1.4. The sensitivity of I^- CIMS to the detection of HO_2 was determined to be a function of the mixing ratio of water in the flow tube as well as the extent of clustering/declustering in the system, e.g. reduction of the I-H_2O^-:I^- ratio due to higher E/N in the declustering region, results in a lower observed sensitivity. Additional work to characterize the effect of humidity on the detection efficiency is necessary to refine the potential of this method for ambient monitoring of $HO_{2.}$

The difficulty of quantitative sampling through an inlet is a significant limitation to the measurement of radicals in the atmosphere. Laboratory experiments were performed to probe the effect of inlet length on sampling of HO_2 radicals produced in N_2. The results are shown in Figure 2a, as the count rate at a given residence time normalized to the count rate at the shortest residence time. This reaction is likely first order in HO_2 therefore a log-linear fit is the most appropriate representation of the data, however the data has been fit using a linear curve for simplicity. HO_2 is lost at a rate of approximately 0.60 s^{-1} in a 6 mm o.d. PFA inlet. Results indicate that the loss of HO_2 is driven not by surface losses, but loss of HO_2 via reaction with residual NO_2 in the system to produce HO_2NO_2, as can be observed in the nearly equivalent rate of increase in observed HO_2NO_2 (0.67 s^{-1}, Figure 2b). Qualitative observations of H_2O_2, at m/z 161 ($I\text{-}H_2O_2^-$), during the same experiment suggest that there is no loss of HO_2 via self-reaction occurring on these timescales.

3.1.2 Peroxy Nitric Acid (HO_2NO_2, PNA)

Two methods were used in this work for the production of a PNA standard. In the first of these methods, PNA was synthesized using the techniques described in Appelman and Gosztola 1995 (Appelman and Gosztola, 1995). Briefly, a nitrite-peroxide solution ($NaNO_2$ in 30% H_2O_2) is mixed with a peroxide-acid solution (30% H_2O_2 in 70% $HClO_4$) at -20 ºC to produce approximately 1.7 M PNA in H_2O_2. The resulting solution is placed in a glass diffusion cell, (Williams et al., 2000), at a temperature of -20 ºC with zero air passed over the headspace to produce a dynamic mixture of PNA. The 20 sccm diffusion source outflow was sampled directly into the inlet flow of the I^- CIMS. This method of synthesis also results in the production of non-negligible amounts of HNO_3 and H_2O_2. While nylon wool can be used to semi-selectively remove HNO_3 from the calibration flow, no method for the selective removal of H_2O_2 was identified. In any case, HNO_3 and H_2O_2 are observed at unique m/z ions and therefore do not interfere with PNA measurement.

Alternatively, PNA can be dynamically generated using the output of the HO_2 source described in section 2.2.1 (Ulrich et al., 2012). Addition of NO_2 to the output of the HO_2 radical source results in the production of PNA. Due to the relative simplicity of this technique, photo-production of PNA was used as the preferred I^- CIMS calibration method for the laboratory and field measurements.

Figure 1 shows a difference mass spectrum of HO_2NO_2 detected using an iodide CIMS instrument with a 'cold' inlet (Figure 1b) and an inlet dissociator temperature of 130ºC (Figure 1c). In both cases, the instrument background was chosen as the ion signal prior to the addition of NO_2. When using a 'cold' inlet, ~30ºC, the dominant peak observed is m/z 62 (NO_3^-), equation 7. An ion signal at m/z 206 ($I\text{-}HO_2NO_2^-$) is also observed, although to a much lesser extent than m/z 62 (NO_3^-), equation 6. When an inlet dissociator is used, HO_2NO_2 is observed at m/z 62 (NO_3^-) and m/z 160 ($I\text{-}HO_2^-$), where the detection of PNA at m/z 62 (NO_3^-) results from incomplete thermal dissociation of HO_2NO_2 in the inlet.

3.1.3 HONO

Similarly to PNA, HONO can be formed by addition of NO to the output of the HO_2 source described in section 3.1.1. Addition of excess NO to the HO_2 calibration source results in the production of HONO from titration of HO_2, as well as any OH produced in the source, via the following reactions:

$$HO_2 + NO \longrightarrow OH + NO_2 \qquad (10)$$

$$OH + NO \longrightarrow HONO \tag{11}$$

Figure 1d shows the difference mass spectrum of the HONO calibration source, where the instrument background here was chosen as the ion signal prior to the addition of NO. It is clear from the figure that HONO is the only product formed and is detected by I^- CIMS at m/z 174 ($I\text{-}HONO^-$). This result is in contrast to the Abida et al. 2011 study which also reports m/z 46 as a minor ion, a difference that can be attributed to the relatively stronger clustering used in our work.

This method of HONO production is instantaneous and does not require the period of stabilization that is necessary for acid-salt reaction based sources (Febo et al., 1995). HONO standard production via the reaction of HO_2 and NO provides a good alternative to previously used I^- CIMS calibration methods (Roberts et al., 2010).

3.2 Dynamic Source Calibration

Quantification of PNA and HONO produced using the above-described methods was performed using the quartz catalysis total NO_y instrument (Wild et al., 2014) , described in section 2.2.2. Laboratory experiments indicate that more than 99% of PNA is thermally dissociated above a temperature of 100 ºC while HONO decomposition is negligible below 200 ºC. The quartz inlet was operated at gas temperatures of 160ºC and 720ºC for the measurement of PNA and HONO, respectively. The difference in total NO_y minus the sum of NO_2 and NO detected yields a quantitative measurement of the PNA or HONO produced in the source.

During these experiments the calibration source flow was alternately sampled by the I^- CIMS and CRD instruments. In order to eliminate any differences in radical reaction times, as a result of inconsistencies in the inlet lengths between the two instruments, the gaseous mixture was passed over glass wool subsequent to addition of NO or NO_2 to terminate the reaction by removing any remaining HO_2 radicals. In this manner the I^- CIMS sensitivity is calculated as the ratio of the I^- CIMS ion signal to the CaRDS measured concentrations. A summary of instrument sensitivities and detections limits (3σ) is included in Table 1. For the calibration data reported in Table 1, the m/z 145 to m/z 127 ratio was approximately 30%.

The I^- CIMS sensitivity towards HONO at the $I\text{-}HONO^-$ cluster (m/z 174), reaction (9), was determined to be 1.7 Hz $ppbv^{-1}$ with a corresponding 3σ instrumental detection limit of 30 pptv. The detection limit for HONO is largely limited by the magnitude of the ever-present $I\text{-}NO_2^-$ (m/z 173) ion and the low resolution of the quadrupole mass spectrometer used in this work. The HONO sensitivity reported here represents detection with a 25ºC inlet, however, the instrument sensitivity was found to be nearly equivalent, within the stated uncertainties, using the heated (130ºC) dissociator.

The sensitivity towards PNA was determined for detection at the $I\text{-}HO_2NO_2^-$ (m/z 206, 25ºC inlet), $I\text{-}HO_2^-$ (m/z 160, 130ºC inlet), and NO_3^- (m/z 62, 25ºC inlet) ions, reactions (6) though (8) respectively. The most sensitive method of detection was observed *via* NO_3^- in a 25ºC inlet, 144 Hz $pptv^{-1}$ with a corresponding 3σ detection limit of 0.7 pptv. Detection at the $I\text{-}HO_2^-$ and $I\text{-}HO_2NO_2^-$ ions are considerably less sensitive, 2.0 and 0.4 Hz $pptv^{-1}$ respectively. The 3σ detection limits are approximately 40 and 20 pptv for $I\text{-}HO_2^-$ and $I\text{-}HO_2NO_2^-$ respectively.

While the most sensitive detection of PNA occurs *via* NO_3^-, there exist several potential interferences that are also observed at that ion, see Table 1 in Wang et al. 2014 (Wang et al., 2014). Considering the sensitivity to PNA detection, relatively low daytime levels of PNA will result in significant signals at m/z 62. In fact, a recent study has suggested that evidence exists for a large daytime source of N_2O_5 detected *via* NO_3^- ion using I^- CIMS measurements (Wang et al., 2014); however, low daytime levels of HO_2NO_2 would also be consistent with observations presented in that work. Unfortunately, detection of PNA at m/z 160 ($I\text{-}HO_2^-$) leads to overlap with HO_2 radical detection at that mass. Therefore, we suggest that m/z 206 ($I\text{-}HO_2NO_2^-$) will yield the most reliable, interference free method of PNA detection for ambient measurements. Increasing the $I\text{-}H_2O$ cluster ratio beyond 30% (this study) should improve the instrument sensitivity towards detection of PNA at the m/z 206 cluster ion.

An indirect calibration was performed for the quantification of the HO_2 source, as no direct HO_2 measurement was readily available. An initial amount of HO_2 radicals are generated and monitored *via* the I^- CIMS operated with a 25ºC inlet. A small amount of NO_2 is then added generating PNA with a corresponding reduction in observed I^- CIMS HO_2 signal. The concentration of HO_2 lost by titration is assumed to be equivalent to the amount of PNA produced in the reaction, as the formation of PNA involves the consumption of one HO_2 radical per molecule. Using the previously described PNA calibration method, the sensitivity can be calculated as the ratio of the reduction in the observed I^- CIMS $I\text{-}HO_2^-$ signal to the NO_y measured PNA concentration. The I^- CIMS detection sensitivity was determined using this method to be 2.6 Hz $pptv^{-1}$ with a corresponding 3σ detection limit of 20 pptv. As it was not the focus of this work, the instrument inlet was not optimized for the sampling of radical species; therefore changes in the inlet design and optimization of the iodide-water cluster distribution in the flow tube could both serve to increase the instrument sensitivity and improve instrument detection limits to levels more appropriate for ambient sampling of HO_2.

4 Uintah Basin Wintertime Ozone Study (UBWOS) Observations

Observations of HO_2NO_2 during the UBWOS 2014 study are shown in Figure 3 for the entire duration of the measurement period. Measurements of the I-$HO_2NO_2^-$ ion using a cold inlet were performed only during the initial and final portion of the study for thirty minutes every hour. Ambient air was sampled through a heated inlet dissociator on alternating 30-minute periods with 'cold' sampling performed on the opposite time periods during the following: Jan. 24 – 30 and Feb. 4 -14. For the remainder of the measurements, Jan. 30 - Feb. 4, ambient air was continuously sampled through a heated dissociator. During sampling periods where the inlet dissociator was used PNA was monitored on m/z 160 (I-HO_2), and during periods of 'cold' sampling *via* m/z 206 (I-HO_2NO_2). It is clear from the correlation plot inset in Figure 3 that both sampling methods ('cold' and hot) agree reasonably well, slope = 0.93, R^2 = 0.785. There does appear to be a positive bias in the m/z 160 observations relative to detection at m/z 206, indicated by a positive intercept and clear disagreement during certain periods shown in the Figure 3 timeseries. One possible explanation is the sensitivity at m/z 160 to ambient HO_2 or HO_2 generated in the inlet as a product of PNA decomposition. Given the length, temperature, and residence time of the inlet used (20m, 30ºC, ~ 4.8 sec), PNA is expected to decompose by approximately 5% prior to sampling. The HO_2 radicals produced as a result of PNA decomposition would likely be detected *via* m/z 160 yet remain unobserved on the m/z 206 ion leading to a positive bias in m/z 160 observations. Additionally from laboratory results presented in Figure 2b, we expect there to be production of HO_2NO_2 in the inlet; however, model approximations of the HO_2 mixing ratio during the 2013 study (15 pptv maximum) yields a maximum formation of HO_2NO_2 in the inlet during peak ozone events of ~ 1% (Edwards et al., 2014).

Aside from the sampling conditions already described, several days of PNA measurements were performed during the 2014 study comparing a short unheated PFA inlet (3m, ambient temperature) and a longer heated inlet (20m, 30ºC). An average reduction of 5% is observed in the PNA mixing ratio when sampling through the longer heated inlet as a result of thermal and perhaps surface assisted decomposition. It is important to note that the data presented here are not corrected for these inlet losses and are therefore considered a lower limit on ambient PNA.

During UBWOS 2013, the I^- CIMS was equipped to monitor PAN compounds using a thermal dissociation inlet, 150ºC. This was done prior to the laboratory work described in this manuscript and neither m/z 160 nor m/z 206 were monitored during the measurement period. However, the NO_3^- ion (m/z 62) was monitored throughout the entire campaign with observed signals exceeding 2e5 counts per second at times. Using the calibration data obtained from the laboratory portion of this work, an approximate PNA concentration was determined for the 2013 UBWOS study, assuming the same NO_3^- (m/z 62) sensitivity as measured during the laboratory calibrations performed after the 2014 study (144 Hz $pptv^{-1}$), corrected for differences in dissociator temperatures and transmission of HO_2NO_2 through the heated inlet tip used during the 2013 study. The error associated with this method was calculated to be approximately 60%, largely due to corrections applied to account for differences in instrument tuning and additional HO_2NO_2 losses due to the different inlet conditions used during the two years.

Figure 4a shows the diurnal average of 2013 I^- CIMS observations of PNA for the entire study. While the average diurnal mixing ratio peaks at 0.5 ppbv, mixing ratios up to 1.5 ppbv were observed during the 2013 study and can be explained by the coincidence of high daytime levels of NO_2 with the low temperatures in the Uintah basin. Similarly to the 2014 measurements, also included in Figure 4a, PNA reaches a peak after solar maximum (~ 15:00 MST) with a minimum observed throughout the night. Concentrations of HO_2NO_2 observed during the 2014 study were significantly lower relative to the 2013 study with a maximum average mixing ratio of 0.1 ppbv. During the 2013 and 2014 study, N_2O_5, a nighttime species and potential interference on the NO_3^- ion, was not observed to contribute to the observed daytime signal.

The PNA mixing ratios observed during the 2013 and 2014 studies are expected for cold conditions with active photochemistry and sufficient NO_x pollution. Displayed in Figure 5 are the conditions necessary to sustain an equilibrium concentration of 1 ppbv PNA with respect to temperature and the mixing ratios of HO_2 and NO_2. The dashed area superimposed on the figure represents the approximate range of conditions encountered during the 2013 study, where HO_2 levels were approximated using model results that describe an ozone event observed during the 2013 study, described below. The Uintah basin provided a unique atmosphere that promotes the formation of PNA for several reasons (1) a strong inversion during the wintertime allows concentrations to build up in the boundary layer over several day periods (2) low ambient temperatures favoring the formation of HO_2NO_2 over thermal decomposition, and (3) radical species propagation, e.g. HO_2 formation, is enhanced due to the active chemistry observed during ozone formation events (Edwards et al., 2014). Lastly, as will be discussed later, the snow surface acts as an important interface serving as both a source and a sink of HO_2NO_2.

The conditions encountered in the basin between the 2013 and 2014 season can be used to explain the large difference in the observed PNA ambient mixing ratios, shown in Figure 4a. Mainly during the 2013 study we observed strong inversions over multi-day periods allowing the buildup of primary and secondary pollutants, a phenomenon driven by snow surface cover and meteorological conditions encountered during the 2013 study (Ahmadov et al., 2015;Edwards et al., 2014). In contrast, relatively low snow cover during the 2014 season limited the formation of multi-day inversions yielding lower ambient mixing ratios of both primary and secondary pollutants. The resulting combination of lower NO_x mixing ratios and higher ambient temperatures during the 2014 study thereby favored thermal dissociation of HO_2NO_2 and led to lower ambient mixing ratios than observed during the 2013 study. In addition, limited snow cover and reduced deposition of NO_y species to the snow surface, as a result of lower ambient mixing ratios, likely reduced the role of the snow surface as a source of HO_2NO_2 in 2014.

As described previously, the vertical gradient of various species was probed through the use of a dual inlet system (18.4m and 1m heights) during the UBWOS 2014 study. A comparison of those measurements for PNA is shown in Figure 4a as diurnal averages of the measurements where dual inlet switching was applied. Figure 4b shows the result of the difference of the 1m minus the 18.4m PNA measurements where the shaded region represents one standard deviation of the average for the entire study. Displayed in this fashion, a positive value is an indication that PNA is larger in the surface coupled layer, characteristic of daytime observations, than aloft with the opposite indicating a relative enhancement of PNA in the layer decoupled from the surface, which was typically observed at night. On average, HO_2NO_2 is depleted at the surface relative to air aloft by approximately 15 pptv with a reversal of nearly the same magnitude observed during midday. It is important to note that this data represents a 1-hour average over the entire six-week measurement period, and while the overall magnitude shown here is small observed ΔPNA values ranged from -150 pptv to 150 pptv.

One interpretation of these results is that deposition of PNA to the snow surface occurs throughout the night in the Uintah Basin with an emission from the snow surface observed in the early morning to midday. Through this mechanism snow surface photolysis of PNA could serve as an additional daytime surface source of NO_2 and HO_2. A similar result has been reported by a recent study (Jones et al., 2014), where evidence for surface exchange was observed for HO_2NO_2 and HNO_3 during the Antarctic winter. However, previous studied have highlighted the complexities of photochemistry chemistry occurring at or directly above snow surfaces (Chen et al., 2007;Chen et al., 2001), which complicates the interpretation of these observations.

Specifically, previous studies have shown enhancements of reactive species integral to HO_x and NO_x budgets at snow surfaces, e.g. HONO, CH_2O, H_2O_2 (Hutterli et al., 1999;Hutterli et al., 2001;Honrath et al., 1999;Ridley et al., 2000;Zhou et al., 2001). Photolysis of these HO_x/NO_x precursors at or above the snow surface or a direct emission of NO_x could result in a net apparent surface source of HO_2NO_2 as it would shift the gas phase equilibrium, reactions (1) and (2), towards the formation of HO_2NO_2. The net effect of this process on the HO_x budget at the snow surface is difficult to quantify without simultaneous observations of the other dominant HO_x precursors and an understanding of their chemical fates. Therefore further validation of our interpretation, a bidirectional flux of HO_2NO_2 from the snow surface, awaits direct flux measurements of HO_2NO_2 over these highly polluted snow surfaces.

Regardless of the underlying mechanisms, the dynamics causing the observed vertical distribution in PNA observations, whether mixing or deposition in origin, can have a measureable impact on the ozone formation potential in the Uintah basin. To investigate the effects, a chemical box model, based on the MCM v3.2 chemistry scheme, has been developed to describe observed ozone production during a wintertime ozone pollution episode during UBWOS 2013 (Edwards et al., 2014). This 0-D model contains a near-explicit oxidation mechanism for 32 observed VOC and oxidized VOC, and is constrained using constant emissions of primary species (VOC and NO), with the concentrations of all other species calculated by the chemistry scheme. Physical loss processes, such as mixing and deposition, are represented via a bimodal 1st order loss process for all species, the rate of which has been optimized based on boundary layer height observations and the concentrations of long lived species, e.g. methane.

Figure 6a and 6b display the base model calculation of PNA and ozone reported in the Edwards et al. 2014 study. While there is reasonable quantitative agreement between the model and measurement daily maxima, there is a temporal shift in PNA measurements relative to model predictions. While the reasons for this are as of yet unknown, possible explanations include underestimation in modeled NO, additional daytime PNA loss mechanisms, or issues with the simple parameterization of mixing used in the model. The latter seems unlikely as the model reproduces the observed diurnal variation in ozone relatively well. As discussed above, there is also evidence that PNA is lost to the snow surface, though the temporal trend in deposition implied from the gradient measurements does not suggest a relatively higher rate in the morning to early afternoon than in the evening, rather there is a possible indication of a mid-day snow surface source. Nitrogen oxides within the model are parameterized using a constant source of NO, with the partitioning of all nitrogen oxides calculated by the chemistry scheme. A quantitative comparison of NO observations to modeled values suggests that the model does typically underestimate the NO concentration throughout the morning. This underestimation would lead to an underestimation of the loss of HO_2 *via* reaction with NO, thereby slowing the formation rate leading to an over-prediction of PNA. This process would have a particular impact in the morning hours where observed NO is relatively large and the HO_2 source is limited.

Deposition of PNA has the potential to result in a net loss of HO_x and thus an increase in NO (Grannas et al., 2007), due to reduced titration to NO_2, which would have an overall effect on ozone formation potential. The sensitivity of ozone production in the UBWOS 2013 box model to changes in the lifetime of PNA with respect to deposition (t_{PNA}) was investigated and the results of these tests are displayed in Figure 6. In addition to the 1st order physical loss term applied to all species, predominantly representing losses due to mixing (Edwards et al., 2014), an additional 1st order loss term for PNA was added to the model scheme to represent deposition. Calculations with a lifetime for PNA with respect to deposition (t_{PNA}) of 1-hour yield approximately a 12% reduction in daily max ozone from the base case where no PNA deposition was included. It is not possible to determine the observed lifetime of PNA with respect to deposition to the snow surface using data from the UBWOS 2013 or 2014 studies; however the measurements and model suggest that surface deposition is occurring with a potentially measureable effect on the ozone production in the Uintah basin.

The post-depositional fate of PNA is also important as this scenario assumes that the loss of PNA to the snow surface is irreversible and thus a net HO_x and NO_x sink. Subsequent snow chemistry resulting in storage and volatilization of HO_x (Jones et al., 2014) or NO_x, has the potential to reduce the magnitude of the effects observed in Figure 6b. If PNA dissolves in an aqueous solution, such as a quasi-liquid layer on the snow surface in the Uintah basin, it can undergo the following dissociation and ionic reactions (Logager and Sehested, 1993;Zhu et al., 1993;Goldstein et al., 2005):

$$HO_2NO_2 \longleftrightarrow HO_2NO_{2(s)} \qquad (12)$$

$$HO_2NO_2 \xleftrightarrow{pKa\sim6} H^+ + O_2NO_2^- \tag{13}$$

$$HO_2NO_{2(s)} \longrightarrow HONO \tag{14}$$

$$O_2NO_2^- \longrightarrow NO_2^- + O_2 \tag{15}$$

$$O_2NO_2^- \longrightarrow NO_2 + O_2^- \tag{16}$$

$$HONO \xleftrightarrow{pKa\sim2.8} H^+ + NO_2^- \tag{17}$$

Previous work has also shown that uptake of PNA to highly acidic surfaces results in reversible uptake, where chemical loss to NO_2^- is negligible (Zhang et al., 1997).

Measurements of snow surface nitrite made during the 2013 and 2014 study are shown in Figure 7(a) and (b), respectively, along with observations of PNA. Two pollution events observed in 2013 were separated by a cleanout event where additional precipitation (indicated by the blue shaded region in figure 7a) accompanied by higher winds and unstable conditions ventilated the basin. The nitrite content of the snow surface generally increases throughout the first event at a rate proportional to the daily increase in PNA mixing ratio until fresh snow is added and nitrite levels drop. Throughout the second event, nitrite levels in the snow surface again build up as ambient PNA levels also increase. We note here that any HO_2NO_2 dissolved in the snow can form NO_2^- with efficiencies as high as 56% depending on pH (Goldstein et al., 2005).

A more detailed look at snow nitrite content shows a generally observed decrease in surface layer concentrations throughout the day, Figure 7c, a result that is consistent with reversible uptake of nitrite. This daytime depletion of snow nitrite could be evidence of the reversible uptake of PNA, interpreted from data shown in Figure 4a, or an indication of the formation and subsequent release of other nitrogen containing species, such as HONO or NO_x, from the snow surface. It is interesting to note that the highest measurements of snow nitrite in a given day typically occur prior to the build up of ambient PNA. This result is consistent with nocturnal uptake of PNA or HONO to the snow surface, as shown in Figure 4b; however, no evidence of this nighttime enrichment is available, as nighttime measurements of snow surface nitrite were not made. Additionally, the extent to which reactions (13) and (15) were occurring, and therefore PNA contributing to snow nitrite content, cannot be approximated as the pH of the snow surface was not measured during this study. Furthermore, while the deposition and potential volatilization of HO_2NO_2 can contribute to the net flux of nitrite at the snow surface, other species such as HNO_3 and HONO are also known to deposit to snow surfaces and should also be considered as part of the net surface nitrogen budget.

Improved measurements of the deposition velocity on snow surfaces of varying acidities and the chemical fate of PNA after deposition is necessary to improve our understanding of the impacts of PNA deposition to HO_x and NO_x budgets. As our model results indicate the post depositional fate of PNA can have a non-negligible impact on ozone formation potential, particularly in cold regions, such as the Uintah basin, where the lifetime of PNA is sufficiently long such that deposition becomes a dominant sink. Considering the similar surface chemistry and influence on radical budgets for atmospheric HONO (VandenBoer et al., 2015), simultaneous measurement must be performed to understand the tropospheric fate of PNA and

HONO species in cold regions and the extent of their involvement in tropospheric HO_x and NO_x budgets.

4 Conclusions

Laboratory studies have been conducted to demonstrate the utility of I^- CIMS as a method for the quantitative detection of HO_2, PNA, and HONO. Methods for the production and calibration of on-line laboratory standards for HO_2, PNA, and HONO have been developed and described above. The I^- CIMS technique offers an unambiguous method with sufficient sensitivity for the detection of PNA in mid latitude tropospheric regions, an area with a general lack of direct observations. Additionally, while it is not fully explored here, the application of I^- CIMS for the direct detection of HO_2 has significant potential for use in future laboratory, chamber, and ambient measurements.

The I^- CIMS instrument was deployed during the 2013 and 2014 UBWOS studies in the Uintah basin, UT during several wintertime ozone events. Field-based experiments illustrate that as a result of the thermal instability of PNA and the potential for formation within inlets, care must be taken to both characterize sampling inlets and minimize residence times in order to perform accurate quantitative measurements. PNA vertical gradient as well as correlation with snow surface nitrite content suggests that deposition, dissociation and ionic reactions of PNA could serve as a large surface nitrite source in the Uintah basin.

Comparison of the 2013 PNA observations to a chemically explicit box model yields quantitative agreement of daily maximum mixing ratios, but with disagreement in the diurnal cycle in late afternoon. Results of this comparison suggest that increased PNA deposition rates lead to an overall decrease in the ozone production potential in the Uintah basin. This result is dependent on the post-depositional fate of PNA, and more studies aimed at improving our understanding of the deposited HO_x and NO_x and photochemistry of NO_y species on snow surfaces are necessary to model this chemistry correctly. Results of this study demonstrate a clear need for further studies of eddy covariance fluxes of PNA, and HONO, from snow surfaces and investigation of subsequent chemistry to improve our understanding of these species as both a source and sink of HO_x and NO_x.

Acknowledgements

The Uintah Basin Winter Ozone Studies were a joint project led and coordinated by the Utah Department of Environmental Quality (UDEQ) and supported by the Uintah Impact Mitigation Special Service District (UIMSSD), the Bureau of Land Management (BLM), the Environmental Protection Agency (EPA) and Utah State University. This work was funded in part by the Western Energy Alliance, and NOAA's Atmospheric Chemistry, Climate and Carbon Cycle program. We thank Questar Energy Products for site preparation and support.

References

Abida, O., Mielke, L. H., and Osthoff, H. D.: Observation of gas-phase peroxynitrous and peroxynitric acid during the photolysis of nitrate in acidified frozen solutions, Chem. Phys. Lett., 511, 187-192, 10.1016/j.cplett.2011.06.055, 2011.

Ahmadov, R., McKeen, S., Trainer, M., Banta, R., Brewer, A., Brown, S., Edwards, P. M., de Gouw, J. A., Frost, G. J., Gilman, J., Helmig, D., Johnson, B., Karion, A., Koss, A., Langford, A., Lerner, B., Olson, J., Oltmans, S., Peischl, J., Petron, G., Pichugina, Y., Roberts, J. M., Ryerson, T., Schnell, R., Senff, C., Sweeney, C., Thompson, C., Veres, P. R., Warneke, C., Wild, R., Williams, E. J., Yuan, B., and Zamora, R.: Understanding high wintertime ozone pollution events in an oil- and natural gas-producing region of the western US, Atmos. Chem. Phys., 15, 411-429, 10.5194/acp-15-411-2015, 2015.

Appelman, E. H., and Gosztola, D. J.: Aqueous Peroxynitric Acid (HOONO2): A Novel Synthesis and Some Chemical and Spectroscopic Properties, Inorganic Chemistry, 34, 4, 1995.

IUPAC Task Group on Atmosperic Chemical Kinetic Data Evaluation: http://iupac.pole-ether.fr.
, access: December 2014, 2004.

Behnke, W., George, C., Scheer, V., and Zetzsch, C.: Production and decay of ClNO2, from the reaction of gaseous N2O5 with NaCl solution: Bulk and aerosol experiments, J. Geophys. Res.-Atmos., 102, 3795-3804, 10.1029/96jd03057, 1997.

Brune, W. H., Tan, D., Faloona, I. F., Jaegle, L., Jacob, D. J., Heikes, B. G., Snow, J., Kondo, Y., Shetter, R., Sachse, G. W., Anderson, B., Gregory, G. L., Vay, S., Singh, H. B., Davis, D. D., Crawford, J. H., and Blake, D. R.: OH and HO2 chemistry in the North Atlantic free troposphere, Geophys. Res. Lett., 26, 3077-3080, 10.1029/1999gl900549, 1999.

Carpenter, L. J., Green, T. J., Mills, G. P., Bauguitte, S., Penkett, S. A., Zanis, P., Schuepbach, E., Schmidbauer, N., Monks, P. S., and Zellweger, C.: Oxidized nitrogen and ozone production efficiencies in the springtime free troposphere over the Alps, J. Geophys. Res.-Atmos., 105, 14547-14559, 10.1029/2000jd900002, 2000.

Chen, G., Davis, D., Crawford, J., Nowak, J. B., Eisele, F., Mauldin, R. L., Tanner, D., Buhr, M., Shetter, R., Lefer, B., Arimoto, R., Hogan, A., and Blake, D.: An investigation of South Pole HOx chemistry: Comparison of model results with ISCAT observations, Geophys. Res. Lett., 28, 3633-3636, 10.1029/2001gl013158, 2001.

Chen, G., Huey, L. G., Crawford, J. H., Olson, J. R., Hutterli, M. A., Sjostedt, S., Tanner, D., Dibb, J., Lefer, B., Blake, N., Davis, D., and Stohl, A.: An assessment of the polar HOx photochemical budget based on 2003 Summit Greenland field observations, Atmos. Environ., 41, 7806-7820, 10.1016/j.atmosenv.2007.06.014, 2007.

Davis, D., Nowak, J. B., Chen, G., Buhr, M., Arimoto, R., Hogan, A., Eisele, F., Mauldin, L., Tanner, D., Shetter, R., Lefer, B., and McMurry, P.: Unexpected high levels of NO observed at South Pole, Geophys. Res. Lett., 28, 3625-3628, 10.1029/2000gl012584, 2001.

Day, D. A., Wooldridge, P. J., Dillon, M. B., Thornton, J. A., and Cohen, R. C.: A thermal dissociation laser-induced fluorescence instrument for in situ detection of NO2, peroxy nitrates, alkyl nitrates, and HNO3, J. Geophys. Res.-Atmos., 107, 10.1029/2001jd000779, 2002.

DeMore, W. B., Sander, S. P., Glolden, G. M., Hampson, R. F., Kurylo, M.J., Howeard, C. J., Ravishankara, A. R., Kolb, C. E., and Molina, M. J.: Chemical kinetics and photochemical data for use in stratospheric modeling, Propulsion Laboratory, Pasadena, CA, 1997.

Dusanter, S., Vimal, D., and Stevens, P. S.: Technical note: Measuring tropospheric OH and HO2 by laser-induced fluorescence at low pressure. A comparison of calibration techniques, Atmos. Chem. Phys., 8, 321-340, 2008.

Edwards, P. M., Brown, S. S., Roberts, J. M., Ahmadov, R., Banta, R. M., deGouw, J. A., Dube, W. P., Field, R. A., Flynn, J. H., Gilman, J. B., Graus, M., Helmig, D., Koss, A., Langford, A. O., Lefer, B. L., Lerner, B. M., Li, R., Li, S. M., McKeen, S. A., Murphy, S. M., Parrish, D. D., Senff, C. J., Soltis, J., Stutz, J., Sweeney, C., Thompson, C. R., Trainer, M. K., Tsai, C., Veres, P. R., Washenfelder, R. A., Warneke, C., Wild, R. J., Young, C. J., Yuan, B., and Zamora, R.: High winter ozone pollution from carbonyl photolysis in an oil and gas basin, Nature, 514, 351-+, 10.1038/nature13767, 2014.

Faloona, I., Tan, D., Brune, W. H., Jaegle, L., Jacob, D. J., Kondo, Y., Koike, M., Chatfield, R., Pueschel, R., Ferry, G., Sachse, G., Vay, S., Anderson, B., Hannon, J., and Fuelberg, H.: Observations of HOx and its relationship with NOx in the upper troposphere during SONEX, J. Geophys. Res.-Atmos., 105, 3771-3783, 10.1029/1999jd900914, 2000.

Febo, A., Perrino, C., Gherardi, M., and Sparapani, R.: Evaluation of a high-purity and high-stability continuous generation system for nitrous acid, Environ. Sci. Technol., 29, 2390-2395, 1995.

Gierczak, T., Jimenez, E., Riffault, V., Burkholder, J. B., and Ravishankara, A. R.: Thermal decomposition of HO2NO2 (peroxynitric acid, PNA): Rate coefficient and determination of the enthalpy of formation, Journal of Physical Chemistry A, 109, 586-596, 10.1021/jp046632f, 2005.

Goldstein, S., Lind, J., and Merenyi, G.: Chemistry of peroxynitrites as compared to peroxynitrates, Chem. Rev., 105, 2457-2470, 10.1021/cr0307087, 2005.

Grannas, A. M., Jones, A. E., Dibb, J., Ammann, M., Anastasio, C., Beine, H. J., Bergin, M., Bottenheim, J., Boxe, C. S., Carver, G., Chen, G., Crawford, J. H., Domine, F., Frey, M. M., Guzman, M. I., Heard, D. E., Helmig, D., Hoffmann, M. R., Honrath, R. E., Huey, L. G., Hutterli, M., Jacobi, H. W., Klan, P., Lefer, B., McConnell, J., Plane, J., Sander, R., Savarino, J., Shepson, P. B., Simpson, W. R., Sodeau, J. R., von Glasow, R., Weller, R., Wolff, E. W., and Zhu, T.: An overview of snow photochemistry: evidence, mechanisms and impacts, Atmos. Chem. Phys., 7, 4329-4373, 2007.

Honrath, R. E., Peterson, M. C., Guo, S., Dibb, J. E., Shepson, P. B., and Campbell, B.: Evidence of NOx production within or upon ice particles in the Greenland snowpack, Geophys. Res. Lett., 26, 695-698, 10.1029/1999gl900077, 1999.

Huey, L. G., Villalta, P. W., Dunlea, E. J., Hanson, D. R., and Howard, C. J.: Reactions of CF3O- with atmospheric trace gases, Journal of Physical Chemistry, 100, 190-194, 10.1021/jp951928u, 1996.

Huey, L. G., Tanner, D. J., Slusher, D. L., Dibb, J. E., Arimoto, R., Chen, G., Davis, D., Buhr, M. P., Nowak, J. B., Mauldin, R. L., Eisele, F. L., and Kosciuch, E.: CIMS measurements of HNO3 and SO2 at the South Pole during ISCAT 2000, Atmos. Environ., 38, 5411-5421, 10.1016/j.atmosenv.2004.04.037, 2004.

Huey, L. G.: Measurement of trace atmospheric species by chemical ionization mass spectrometry: Speciation of reactive nitrogen and future directions, Mass Spec. Rev., 26, 166-184, 10.1002/mas.20118, 2007.

Hutterli, M. A., Rothlisberger, R., and Bales, R. C.: Atmosphere-to-snow-to-firn transfer studies of HCHO at Summit, Greenland, Geophys. Res. Lett., 26, 1691-1694, 10.1029/1999gl900327, 1999.

Hutterli, M. A., McConnell, J. R., Stewart, R. W., Jacobi, H. W., and Bales, R. C.: Impact of temperature-driven cycling of hydrogen peroxide (H2O2) between air and snow on the planetary boundary layer, J. Geophys. Res.-Atmos., 106, 15395-15404, 10.1029/2001jd900102, 2001.

Jimenez, E., Gierczak, T., Stark, H., Burkholder, J. B., and Ravishankara, A. R.: Reaction of OH with HO2NO2 (peroxynitric acid): Rate coefficients between 218 and 335 K and product yields at 298 K, Journal of Physical Chemistry A, 108, 1139-1149, 10.1021/jp0363489, 2004.

Jimenez, E., Gierczak, T., Stark, H., Burkholder, J. B., and Ravishankara, A. R.: Quantum yields of OH, HO2 and NO3 in the UV photolysis of HO2NO2, Phys. Chem. Chem. Phys., 7, 342-348, 10.1039/b413429j, 2005.

Jones, A. E., Brough, N., Anderson, P. S., and Wolff, E. W.: HO2NO2 and HNO3 in the coastal Antarctic winter night: a "lab-in-the-field" experiment, Atmos. Chem. Phys., 14, 11843-11851, 10.5194/acp-14-11843-2014, 2014.

Keim, C., Liu, G. Y., Blom, C. E., Fischer, H., Gulde, T., Hopfner, M., Piesch, C., Ravegnani, F., Roiger, A., Schlager, H., and Sitnikov, N.: Vertical profile of peroxyacetyl nitrate (PAN) from MIPAS-STR measurements over Brazil in February 2005 and its contribution to tropical UT NO(y) partitioning, Atmos. Chem. Phys., 8, 4891-4902, 2008.

Kim, S., Huey, L. G., Stickel, R. E., Tanner, D. J., Crawford, J. H., Olson, J. R., Chen, G., Brune, W. H., Ren, X., Lesher, R., Wooldridge, P. J., Bertram, T. H., Perring, A., Cohen, R. C., Lefer, B. L., Shetter, R. E., Avery, M., Diskin, G., and Sokolik, I.: Measurement of HO2NO2 in the free troposphere during the intercontinental chemical transport experiment - North America 2004, J. Geophys. Res.-Atmos., 112, 10.1029/2006jd007676, 2007.

Lee, B. H., Lopez-Hilfiker, F. D., Mohr, C., Kurten, T., Worsnop, D. R., and Thornton, J. A.: An Iodide-Adduct High-Resolution Time-of-Flight Chemical-Ionization Mass Spectrometer: Application to Atmospheric Inorganic and Organic Compounds, Environ. Sci. Technol., 48, 6309-6317, 10.1021/es500362a, 2014.

Li, Z. J., Friedl, R. R., Moore, S. B., and Sander, S. P.: Interaction of peroxynitric acid with solid H2O ice, J. Geophys. Res.-Atmos., 101, 6795-6802, 10.1029/96jd00065, 1996.

Logager, T., and Sehested, K.: Formation and decay of peroxtnitric acid - A pulse-radiolysis study Journal of Physical Chemistry, 97, 10047-10052, 1993.

Lyman, S., and Shorthill, H.: Final Report: 2012 Uintah Basin Winter Ozone & Air Quality Study, Utah State University, 281, 2012.

Murphy, J. G., Thornton, J. A., Wooldridge, P. J., Day, D. A., Rosen, R. S., Cantrell, C., Shetter, R. E., Lefer, B., and Cohen, R. C.: Measurements of the sum of HO2NO2 and CH3O2NO2 in the remote troposphere, Atmos. Chem. Phys., 4, 377-384, 2004.

Niki, H., Maker, P. D., Savage, C. M., and Breitenbach, L. P.: Fourier-Transform IR spectroscopy observation of pernitric acid formed via HOO + NO2 -> HOONO2, Chem. Phys. Lett., 45, 564-566, 10.1016/0009-2614(77)80090-0, 1977.

Ridley, B., Walega, J., Montzka, D., Grahek, F., Atlas, E., Flocke, F., Stroud, V., Deary, J., Gallant, A., Boudries, H., Bottenheim, J., Anlauf, K., Worthy, D., Sumner, A. L., Splawn, B., and Shepson, P.: Is the Arctic surface layer a source and sink of NOx in winter/spring?, J. Atmos. Chem., 36, 1-22, 10.1023/a:1006301029874, 2000.

Rinsland, C. P., Zander, R., Farmer, C. B., Norton, R. H., Brown, L. R., Russell, J. M., and Park, J. H.: Evidence for the presence of the 802.7 cm-1 band Q branch of HO2NO2 in high-resolution solar absorption spectra of the stratosphere, Geophys. Res. Lett., 13, 761-764, 10.1029/GL013i008p00761, 1986.

Rinsland, C. P., Gunson, M. R., Salawitch, R. J., Michelsen, H. A., Zander, R., Newchurch, M. J., Abbas, M. M., Abrams, M. C., Manney, G. L., Chang, A. Y., Irion, F. W., Goldman, A., and Mahieu, E.: ATMOS/ATLAS-3 measurements of stratospheric chlorine and reactive nitrogen partitioning inside and outside the November 1994 Antarctic vortex, Geophys. Res. Lett., 23, 2365-2368, 10.1029/96gl01474, 1996.

Roberts, J. M., Veres, P., Warneke, C., Neuman, J. A., Washenfelder, R. A., Brown, S. S., Baasandorj, M., Burkholder, J. B., Burling, I. R., Johnson, T. J., Yokelson, R. J., and de Gouw, J.: Measurement of HONO, HNCO, and other inorganic acids by negative-ion proton-transfer chemical-ionization mass spectrometry (NI-PT-CIMS): application to biomass burning emissions, Atmos. Meas. Tech., 3, 981-990, 10.5194/amt-3-981-2010, 2010.

Roehl, C. M., Nizkorodov, S. A., Zhang, H., Blake, G. A., and Wennberg, P. O.: Photodissociation of peroxynitric acid in the near-IR, Journal of Physical Chemistry A, 106, 3766-3772, 10.1021/jp013536v, 2002.

Salawitch, R. J., Wennberg, P. O., Toon, G. C., Sen, B., and Blavier, J. F.: Near IR photolysis of HO2NO2: Implications for HOx, Geophys. Res. Lett., 29, 10.1029/2002gl015006, 2002.

Chemical Kinetics and Photochemical Data for Use in Atmospheric Studies: http://jpldataeval.jpl.nana.gov, access: 10-6, 2011.

Sen, B., Toon, G. C., Osterman, G. B., Blavier, J. F., Margitan, J. J., Salawitch, R. J., and Yue, G. K.: Measurements of reactive nitrogen in the stratosphere, J. Geophys. Res.-Atmos., 103, 3571-3585, 10.1029/97jd02468, 1998.

Singh, H. B., Brune, W. H., Crawford, J. H., Jacob, D. J., and Russell, P. B.: Overview of the summer 2004 intercontinental chemical transport experiment - North America (INTEX-A), J. Geophys. Res.-Atmos., 111, 10.1029/2006jd007905, 2006.

Singh, H. B., Salas, L., Herlth, D., Kolyer, R., Czech, E., Avery, M., Crawford, J. H., Pierce, R. B., Sachse, G. W., Blake, D. R., Cohen, R. C., Bertram, T. H., Perring, A., Wooldridge, P. J., Dibb, J., Huey, G., Hudman, R. C., Turquety, S., Emmons, L. K., Flocke, F., Tang, Y., Carmichael, G. R., and Horowitz, L. W.: Reactive nitrogen distribution and partitioning in the North American troposphere and lowermost stratosphere, J. Geophys. Res.-Atmos., 112, 10.1029/2006jd007664, 2007.

Slusher, D. L., Pitteri, S. J., Haman, B. J., Tanner, D. J., and Huey, L. G.: A chemical ionization technique for measurement of pernitric acid in the upper troposphere and the polar boundary layer, Geophys. Res. Lett., 28, 3875-3878, 10.1029/2001gl013443, 2001.

Slusher, D. L., Huey, L. G., Tanner, D. J., Chen, G., Davis, D. D., Buhr, M., Nowak, J. B., Eisele, F. L., Kosciuch, E., Mauldin, R. L., Lefer, B. L., Shetter, R. E., and Dibb, J. E.: Measurements of pernitric acid at the South Pole during ISCAT 2000, Geophys. Res. Lett., 29, 10.1029/2002gl015703, 2002.

Slusher, D. L., Huey, L. G., Tanner, D. J., Flocke, F. M., and Roberts, J. M.: A thermal dissociation-chemical ionization mass spectrometry (TD-CIMS) technique for the simultaneous measurement of peroxyacyl nitrates and dintrogen pentoxide, J. Geophys. Res.-Atmos., 109, D19315, doi:10.1029/2004JD004670, 2004.

Slusher, D. L., Neff, W. D., Kim, S., Huey, L. G., Wang, Y., Zeng, T., Tanner, D. J., Blake, D. R., Beyersdorf, A., Lefer, B. L., Crawford, J. H., Eisele, F. L., Mauldin, R. L., Kosciuch, E., Buhr, M.

P., Wallace, H. W., and Davis, D. D.: Atmospheric chemistry results from the ANTCI 2005 Antarctic plateau airborne study, J. Geophys. Res.-Atmos., 115, 10.1029/2009jd012605, 2010.

Spencer, K. M., McCabe, D. C., Crounse, J. D., Olson, J. R., Crawford, J. H., Weinheimer, A. J., Knapp, D. J., Montzka, D. D., Cantrell, C. A., Hornbrook, R. S., Mauldin, R. L., and Wennberg, P. O.: Inferring ozone production in an urban atmosphere using measurements of peroxynitric acid, Atmos. Chem. Phys., 9, 3697-3707, 2009.

Stark, H., Brown, S. S., Burkholder, J. B., Aldener, M., Riffault, V., Gierczak, T., and Ravishankara, A. R.: Overtone dissociation of peroxynitric acid (HO2NO2): Absorption cross sections and photolysis products, Journal of Physical Chemistry A, 112, 9296-9303, 10.1021/jp802259z, 2008.

Final Report 2013 Uinta Basin Winter Ozone Study: http://www.deq.utah.gov/locations/U/uintahbasin/studies/UBOS-2013.htm, access: July, 2014.

Ulrich, T., Ammann, M., Leutwyler, S., and Bartels-Rausch, T.: The adsorption of peroxynitric acid on ice between 230 K and 253 K, Atmos. Chem. Phys., 12, 1833-1845, 10.5194/acp-12-1833-2012, 2012.

VandenBoer, T. C., Young, C. J., Talukdar, R. K., Markovic, M. Z., Brown, S. S., Roberts, J. M., and Murphy, J. G.: Nocturnal loss and daytime source of nitrous acid through reactive uptake and displacement, Nature Geosci, 8, 55-60, 10.1038/ngeo2298 http://www.nature.com/ngeo/journal/v8/n1/abs/ngeo2298.html - supplementary-information, 2015.

Wang, X., Wang, T., Yan, C., Tham, Y. J., Xue, L., Xu, Z., and Zha, Q.: Large daytime signals of N2O5 and NO3 inferred at 62 amu in a TD-CIMS: chemical interference or a real atmospheric phenomenon?, Atmos. Meas. Tech., 7, 1-12, 10.5194/amt-7-1-2014, 2014.

Wennberg, P. O., Salawitch, R. J., Donaldson, D. J., Hanisco, T. F., Lanzendorf, E. J., Perkins, K. K., Lloyd, S. A., Vaida, V., Gao, R. S., Hintsa, E. J., Cohen, R. C., Swartz, W. H., Kusterer, T. L., and Anderson, D. E.: Twilight observations suggest unknown sources of HOx, Geophys. Res. Lett., 26, 1373-1376, 10.1029/1999gl900255, 1999.

Wild, R., Edwards, P., Dube, W. P., Baumann, K., Edgerton, E. S., Quinn, P. Q., Roberts, J. M., Rollins, A. W., Veres, P. R., Warneke, C., WIlliams, E. J., Yuan, B., and Brown, S.: A Measurement of Total Reactive Nitrogen, NOy, together with NO2, NO, and O3 via Cavity Ring-down Spectroscopy., In Preparation, 2014.

Williams, J., Roberts, J. M., Bertman, S. B., Stroud, C. A., Fehsenfeld, F. C., Baumann, K., Buhr, M. P., Knapp, K., Murphy, P. C., Nowick, M., and Williams, E. J.: A method for the airborne measurement of PAN, PPN, and MPAN, J. Geophys. Res.-Atmos., 105, 28943-28960, 2000.

Wooldridge, P. J., Perring, A. E., Bertram, T. H., Flocke, F. M., Roberts, J. M., Singh, H. B., Huey, L. G., Thornton, J. A., Wolfe, G. M., Murphy, J. G., Fry, J. L., Rollins, A. W., LaFranchi, B. W., and Cohen, R. C.: Total Peroxy Nitrates (Sigma PNs) in the atmosphere: the Thermal Dissociation-Laser Induced Fluorescence (TD-LIF) technique and comparisons to speciated PAN measurements, Atmos. Meas. Tech., 3, 593-607, 10.5194/amt-3-593-2010, 2010.

Zhang, R. Y., Leu, M. T., and Keyser, L. F.: Heterogeneous chemistry of HO2NO2 in liquid sulfuric acid, Journal of Physical Chemistry A, 101, 3324-3330, 10.1021/jp963321z, 1997.

Zhou, X. L., Beine, H. J., Honrath, R. E., Fuentes, J. D., Simpson, W., Shepson, P. B., and Bottenheim, J. W.: Snowpack photochemical production of HONO: a major source of OH in the Arctic boundary layer in springtime, Geophys. Res. Lett., 28, 4087-4090, 10.1029/2001gl013531, 2001.

Zhu, T., Yarwood, G., Chen, J., and Niki, H.: Evidence for the heterogeneous formation of nitrous acid from peroxynitric acid in environmental chambers, Environ. Sci. Technol., 27, 982-983, 10.1021/es00042a024, 1993.

Table 1. Summary of observed products, sensitivities, and detection limits (DL) for the reaction of I^- with HO_2NO_2, HONO and HO_2.

Analyte	Detected Ion (m/z)	Sensitivity[a] (Hz $pptv^{-1}$)	DL (pptv, 3σ)	Inlet[a]
HO_2NO_2	$I\text{-}HO_2NO_2^-$ (206)	0.40 ± 0.06	20	Cold
	NO_3^- (62)	144 ± 11[b]	0.7	Cold, Hot
	$I\text{-}HO_2^-$ (160)	2.0 ± 0.04	40	Hot
HONO	$I\text{-}HONO^-$ (174)	1.7 ± 0.3	30	Cold, Hot
HO_2	$I\text{-}HO_2^-$ (160)	2.6 ± 0.3	20	Cold, Hot

[a] Indicates the inlet dissociation temperature at which the particular ion can be sensitively observed. The inlet dissociator was operated at a temperature of 130ºC (Hot) or at ambient temperature (Cold).

[b] Sensitivity reported is for detection with an inlet dissociator at ambient temperature (Cold).

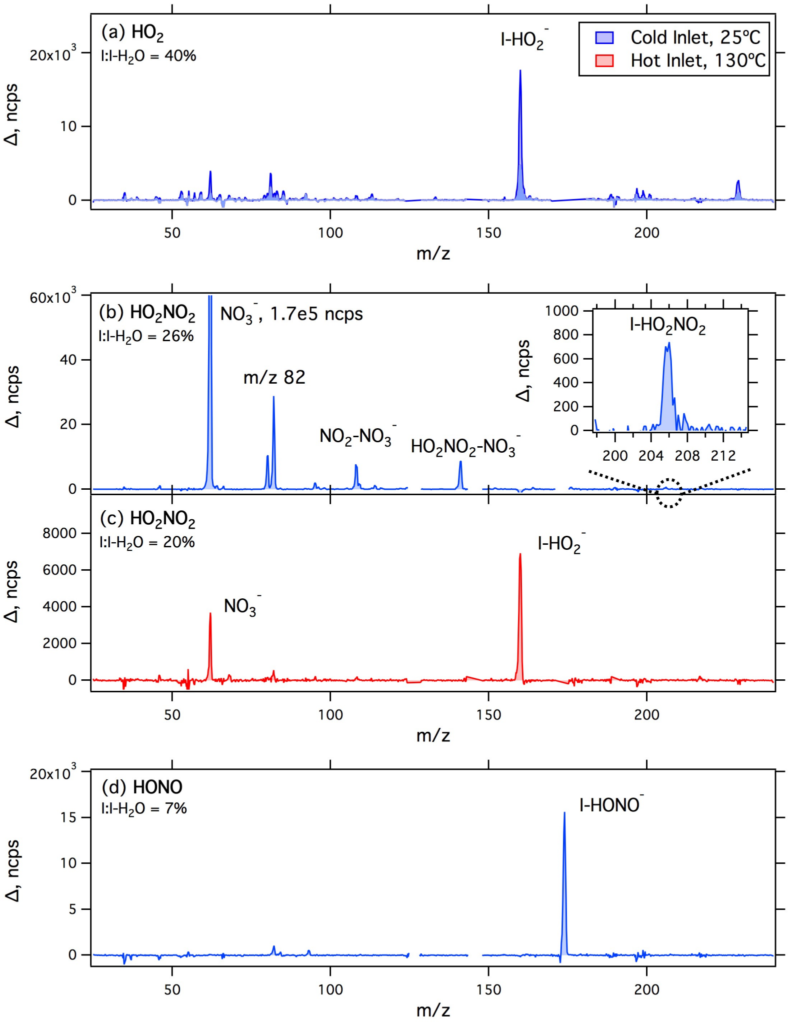

Figure 1. Shown are normalized (1e6 cps I^-), background corrected mass spectra acquired in the laboratory for calibration sources of HO_2 (a), HO_2NO_2 (b) and (c), and HONO (d). Spectra colored in blue were collected using a room temperature inlet (~25ºC) while spectra in red indicate that an inlet dissociator at a temperature of 130ºC was used. Background mass spectra have been subtracted from the displayed mass spectra to highlight the m/z ions that are produced *via* the I^- CIMS ion chemistry. All three species are detectable at a unique m/z, when an inlet dissociator is not used, allowing for simultaneous detection of HO_2, HO_2NO_2, and HONO.

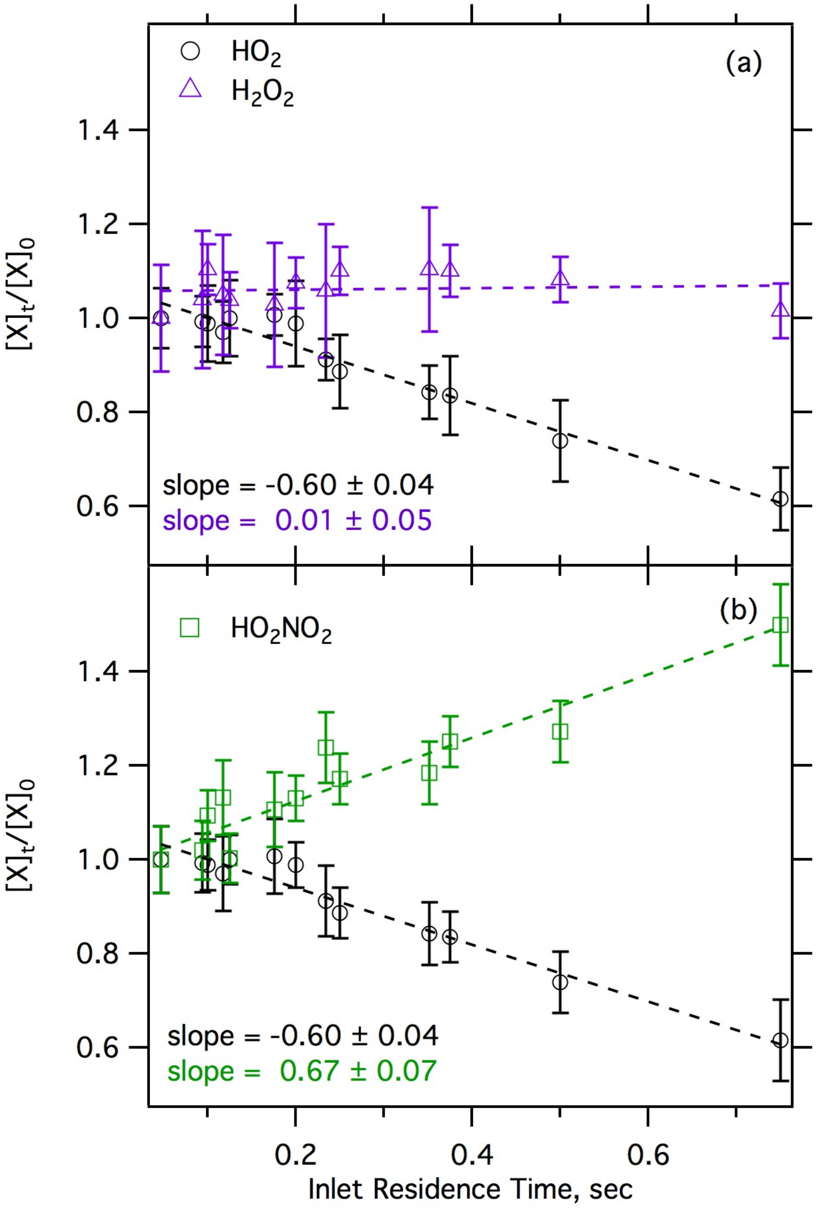

Figure 2. Observed losses versus inlet residence times for a generated standard of HO_2 radicals sampled through PFA tubing at various flow rates (3-6 slpm) and lengths (0-3m). Concentrations have been normalized to the initial concentration observed at the minimum reaction time displayed. Reaction with NO_2 to form HO_2NO_2 appears to be the dominant loss for HO_2 on these timescales.

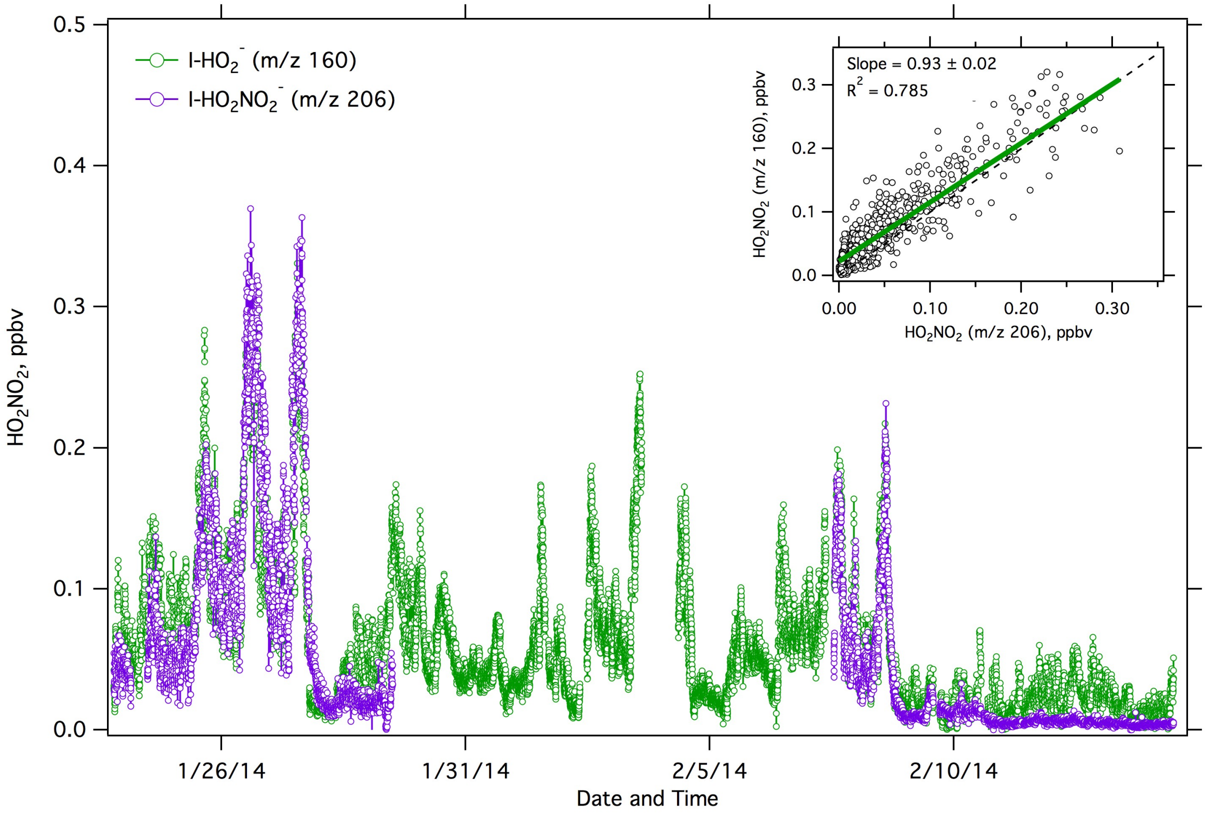

Figure 3. A comparison of HO_2NO_2 observations made using the I-HO_2^- (m/z 160) ion with a hot dissociator (130ºC) and the I-$HO_2NO_2^-$ (m/z 206) ion with a cold dissociator (~25ºC). Inset is a correlation plot of the two measurements where comparison is possible.

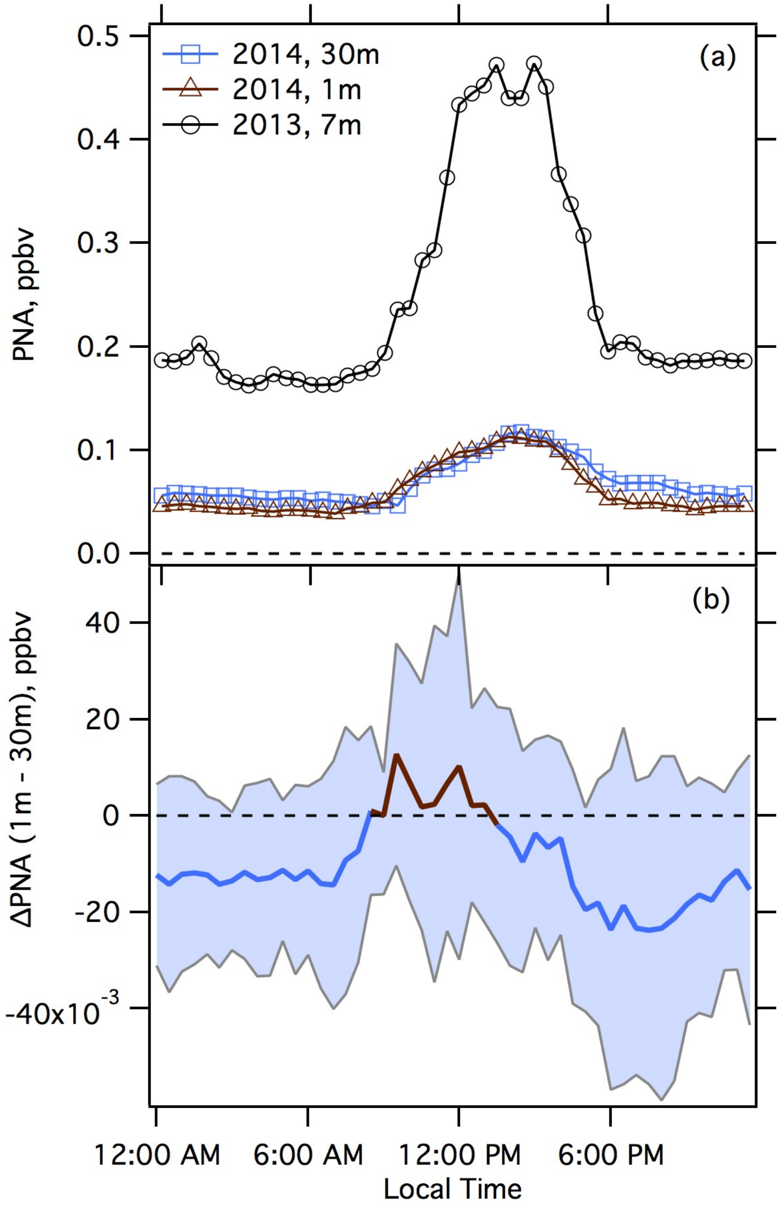

Figure 4. Diurnal profiles of PNA are shown in panel (a) for the full measurement period during the UBWOS 2013 and 2014 studies, with the 2014 study separated based on the sampling height location. Panel (b) presents the difference in the 1m and 18.4m PNA measurements for duration of the 2014 study, where a positive value (brown) indicates larger concentrations at the ground and a negative value (blue) suggests a relative PNA depletion in the 1m measurements. The

shaded region represents 1 standard deviation on the hourly average for the entire measurement period.

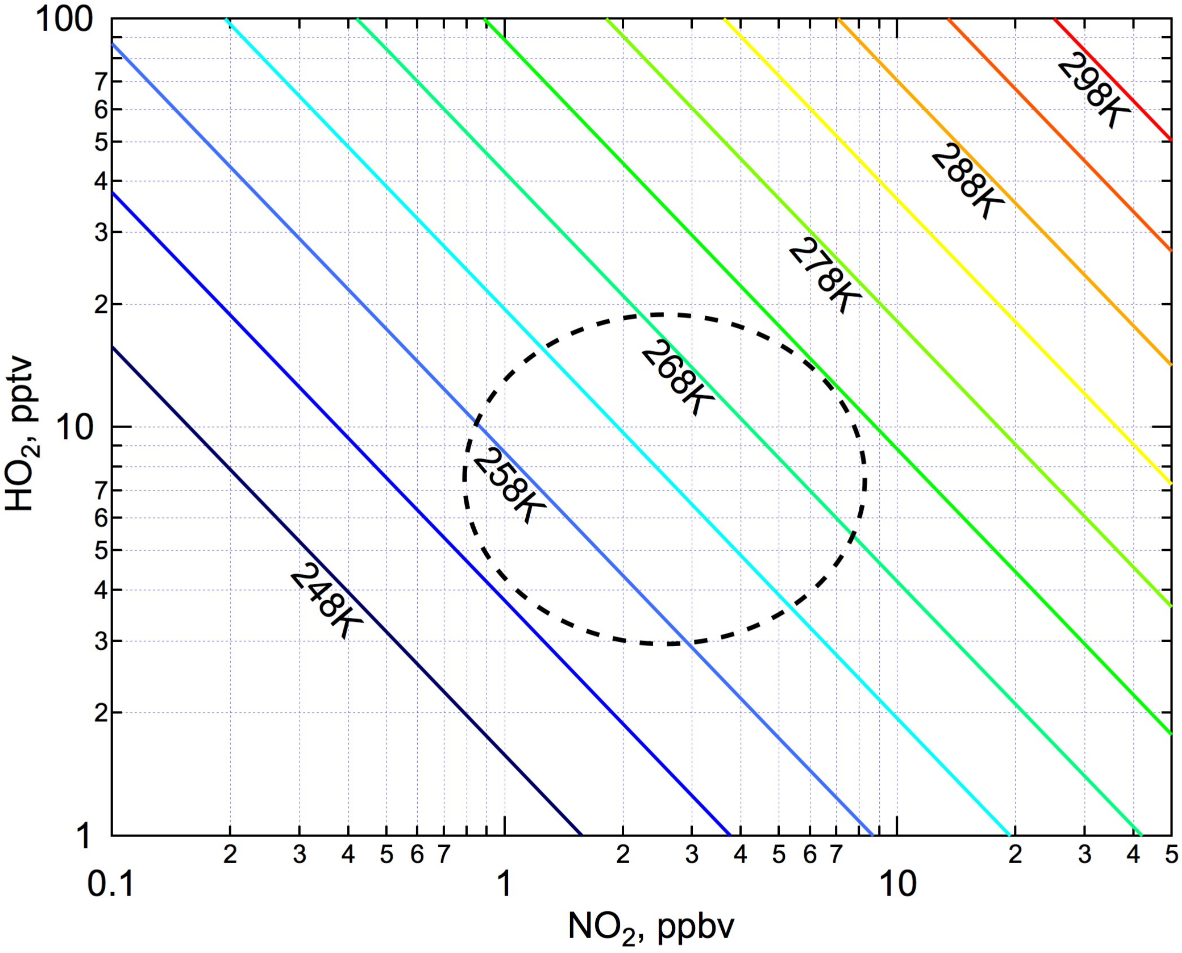

Figure 5. Temperature and mixing ratios of HO_2 and NO_2 required to sustain an equilibrium concentration of 1 ppbv HO_2NO_2. The region within the dashed circle superimposed on the figure highlights the conditions encountered during the 2013 UBWOS study. Data shown were calculated using the IUPAC database (Atkinson et al., 2004).

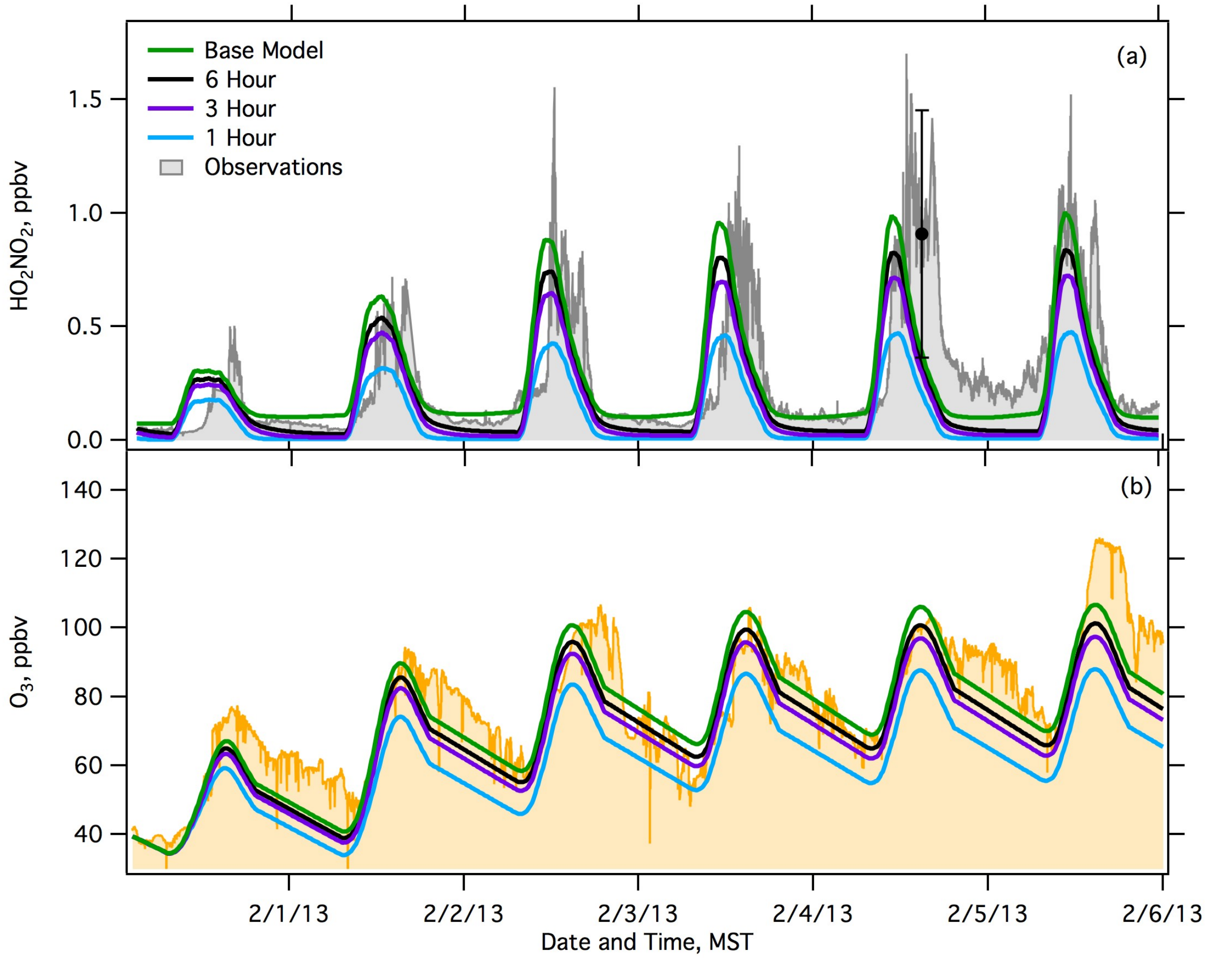

Figure 6. Comparison of PNA and ozone observations throughout an ozone formation event observed during UBWOS 2013 and corresponding model predictions using an explicit chemical box model describing the chemistry. Panel (a), HO_2NO_2 observations compared to model results applying various PNA lifetimes with respect to deposition (t_{PNA}). The datum shown with error bars, black circle, represents the approximated 60% error on the 2013 HO_2NO_2 I^- CIMS measurements. Panel (b) illustrates the effect varying deposition rates of PNA has on total predicted ozone production.

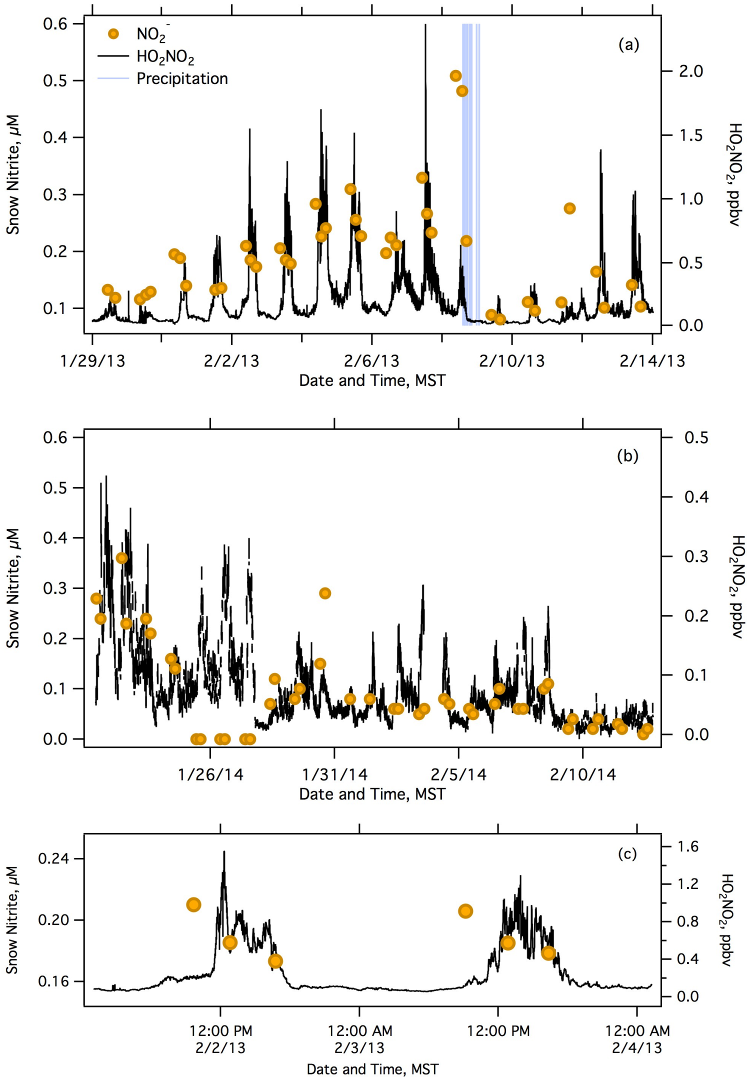

Figure 7. Displayed are gas phase HO_2NO_2 observations made during two wintertime ozone events in the Uintah Basin, UT observed in 2013 (a), and through the entire 2014 study (b). Measurements of the nitrite content of the snow surface taken during the same time periods are also shown. In 2013, a precipitation event that occurred on the afternoon of February 8, shown as the period in blue, added fresh surface snow and flushed pollutants out of the basin resulting in lower ambient PNA and snow nitrite levels. Panel (c) shows in more detail periods from the 2013 measurements to better illustrate the daily reduction in snow surface nitrate that was regularly observed.